Nano World Journal

https://doi.org/10.17756/nwj.2022-s1-008

Research Article

Open Access

Effect of $Ni(NO_3)_2.6H_2O$ Molarity Variation on the Properties of $Ni(OH)_2$ Nanoparticles

Anshu Soni[1], Harish[1], Akash[1], Jyoti Kumari[1], Nitesh Kumar Poddar[2], Rahul Singhal[3], Anoop Kumar Mukhopadhyay[4], and Pushpendra Kumar[1*]

[1]*Department of Physics, Manipal University Jaipur, Rajasthan, India*

[2]*Department of Biosciences, Manipal University Jaipur, Rajasthan, India*

[3]*Department of Physics, Malaviya National Institute of Technology Jaipur, Rajasthan, India*

[4]*Department of Physics, Sharda School of Basic Sciences, Sharda University, Greater Noida, Gautam Buddha Nagar 201310, Uttar Pradesh, India*

***Correspondence to:**
Pushpendra Kumar
Department of Physics, Manipal University
Jaipur, Rajasthan, India
E-mail: pushpendra.kumar@jaipur.manipal.edu

Received: August 23, 2022
Accepted: October 11, 2022
Published: October 12, 2022

Citation: Soni A, Harish, Akash, Kumari J, Poddar NK, et al. 2022. Effect of $Ni(NO_3)_2.6H_2O$ Molarity Variation on the Properties of $Ni(OH)_2$ Nanoparticles. *NanoWorld J* 8(S1): S39-S44.

Copyright: © 2022. Soni et al. This is an Open Access article distributed under the terms of the Creative Commons Attribution 4.0 International License (CC-BY) (http:// creativecommons.org/licenses/by/4.0/) which permits commercial use, including reproduction, adaptation, anddistribution of the article provided the original author and source are credited.

Published by United Scientific Group

Abstract

Nickel hydroxide ($Ni(OH)_2$) is a very significant material from fundamental as well as technological application points of views. It has several technological applications in engineering, particularly it is used as the active material in the positive electrode of rechargeable batteries. It is also used as a common precursor for synthesizing hydrogenation catalyst nickel oxide. The aqueous solution of nickel nitrate hexahydrate ($Ni(NO_3)_2.6H_2O$) and sodium hydroxide (NaOH) are used as precursor. In this report, we have synthesized $Ni(OH)_2$ nanoparticles (NPs) using a simple chemical precipitation method and varied the molarity of $Ni(NO_3)_2.6H_2O$ precursor as 0.4, 0.6, and 0.8 M. The synthesized $Ni(OH)_2$ NPs was studied using several characterizations. From XRD analysis, with the increase of molarity of $Ni(NO_3)_2.6H_2O$ the average crystallite size was found to be increased. Accordingly with the increase in average crystallite size, the bandgap of prepared $Ni(OH)_2$ decreases from 2.66 eV to 2.58 eV. The change in physical properties of prepared $Ni(OH)_2$ NPs was discussed in terms of the molarity variation of the solution. The present study reports the change in physical properties of $Ni(OH)_2$ by change in basic synthesis parameter and the reported results might be useful to assess the material as an active electrode to improve the performance of batteries.

Keywords

Nickel hydroxide, Nickel nitrate, Molarity

Introduction

Nickel hydroxide ($Ni(OH)_2$) has drawn extensive attention of researchers from both fundamental as well technological points of views. The material has its own importance due to its wide range of applications in portable electronics and electric vehicle sensors, supercapacitors, catalysts, and batteries [1, 2]. The huge use of $Ni(OH)_2$ especially in energy storage has forced research to prepare the material by different synthesis processes to have optimized properties for the respective applications. Several synthesis processes was used to prepare this material by researchers around the world. These synthesis methods include a simple chemical precipitation process, microwave-assisted synthesis, solvothermal synthesis, sol-gel synthesis, electrochemical synthesis, hydrothermal synthesis, and sonochemical methods [1, 3, 4]. The main requirement of electrode material for high energy storage are large specific surface area, long durability, low price, high electrical conductivity, resistive to the electrolyte, environment friendly, etc. Several other materials are also used for electrode material including nano porous

carbon, layered transition metal hydroxides, and sulfides [1-4]. However, $Ni(OH)_2$ as an electrode material has been attractive material due to its structural and electronic properties. $Ni(OH)_2$ depending on the synthesis process can have both phases i.e., α- $Ni(OH)_2$ and β-$Ni(OH)_2$ phases [5]. $Ni(OH)_2$ has a hexagonal brucite-type structure and can have layers arranged along the 'c' crystallographic axis. The layered structure of $Ni(OH)_2$ makes this material a choiced of electrode material as the ions can be intercalated between the layers [6, 7]. The synthesis parameters and synthesis methods are important factors for obtaining an electrode material with high performance. Hall *et al.* [1] in their review paper have discussed in detail the types of synthesis methods for obtaining the optimized electrode. In the same review, the different types of disorders or defects that include stacking fault disorder, mechanical stress, hydration and the typic of ionic impurities have been discussed. Furthermore, the various type of physical properties of $Ni(OH)_2$ e.g., mechanical, optical, electrical, and magnetic properties has been discussed in detail and concluded with the optimized method to obtain the material with desired properties. As seen from the literature that the physical properties can be controlled by the type of synthesis process and by varying the synthesis parameters. However, still, there is a gap of knowledge in the literature about the study of basic synthesis parameters that might drastically change the properties of the material for desired application. Hence, this makes the scope of the current study. In the present work, we have used a simple chemical precipitation method and varied the molarity of one of the precursors to study the change in physical properties of synthesis $Ni(OH)_2$ material. The synthesized material was characterized using X-ray diffraction (XRD), Field emission scanning electron microscope (FESEM), Fourier transform infrared spectroscopy (FTIR) and Ultraviolet-Visible (UV-Vis) is spectroscopy.

Material and Methods

$Ni(OH)_2$ NPs were synthesized by dropwise additions of 0.6 M NaOH (AG, 99 %, Sigma Aldrich) solution to an aqueous solution of $Ni(NO_3)_2.6H_2O$ of different molarities i.e.,0.4 M, 1.0 M, 1.6 M as the precipitator while maintaining constant magnetic stirring at 1200 rpm and a temperature of 27 °C. The white precipitate which had accumulated at the bottom of the solution was collected with the help of Whatman 40 filter paper (GE Healthcare UK Limited, UK) after approximately 60 minutes. The precipitate was then washed with deionized water 4-5 times to remove the $NaNO_3$ residues. The resulting precipitate was further heated at 60 °C for 2 hours in a programmable vacuum furnace at which the temperature was raised at a rate of 1 °C/min. Three samples of $Ni(OH)_2$ were prepared by following the previously mentioned synthesis process using $Ni(NO_3)_2.6H_2O$ with varying molarities of 0.4 M, 1.0 M, and 1.6 M, and these powder samples were given the sample names A, B, and C, respectively.

The synthesized $Ni(OH)_2$ powder samples were analyzed using XRD (Malvern Panalytical, Netherlands, Cu K_α λ=0.15406 nm, 30 mA, 40 kV, 10°< 2θ< 80°, scanning rate 0.02°/s), FESEM and EDX (JEOL-7610F, Jeol, Japan), FTIR (Bruker Alpha, USA; 500-4000 cm^{-1}), and UV-Vis (Shimadzu UV-NIR 2600, Japan). The standard Tauc's plots have been used to measure the direct optical energy band gap (Eg) values.

Results and Discussion

Structural analysis

The XRD pattern for $Ni(OH)_2$ powder samples has several peaks, as seen in Figure 1, showing that the synthesized compound is polycrystalline in nature. The $Ni(OH)_2$ crystalline phase is confirmed in all the samples by the diffraction peaks with the indices (001), (002), (100), (110), and (300) at varied 2θ values. The primary peak (001), which was found at 2θ ~12° [8], of the hexagonal β-$Ni(OH)_2$ nanostructures (JCPDS card, No. 22-0444), matches the observed diffraction peak exactly. In all three samples, XRD has been used to identify the pure phase of β-$Ni(OH)_2$ powder, and as shown in Figure 1, no peaks resulting from impurities, or the α-$Ni(OH)_2$ phase were found.

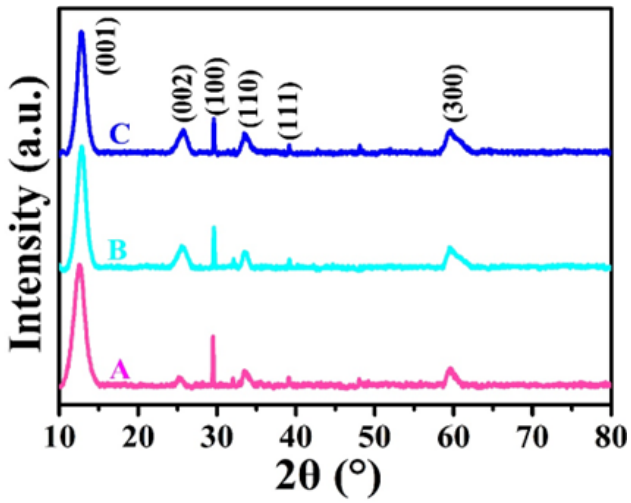

Figure 1: XRD patterns of the samples A, B, and C.

The Scherrer equation was used to calculate the average crystallite size (t_{D-S}) of the samples [9].

$$t_{DS} = \frac{k\lambda}{\beta_{hkl}\,\mathrm{Cos}\,\theta_{hkl}} \qquad \ldots\ldots\ldots\ldots (1)$$

Here k is a correction factor normally taken as 0.9, λ, β, and θ are wavelength, full width at half maxima (FWHM) for particular peak, and angle of diffraction, respectively. Table 1 illustrates the values for average crystallite sizes obtained from equation (1). The result shows that the synthesized ma-

Table 1: Structural and optical characterization results of samples A, B, and C.

Sample	Average crystallite size, t_{D-S} (nm)	Average crystallite size, t_{W-H} (nm)	Strain (ε)
A	16.53	4.10	-0.0139
B	17.49	5.41	-0.0092
C	23.99	10.91	0.0025

terial is nanocrystalline in nature. Secondly, as the molarity of $Ni(NO_3)_2.6H_2O$ precursor increases, the average size of the crystallites in the synthesized powder increases.

In addition, using the sin θ dependent FWHM intensity β of the diffraction lines, the Williamson-Hall (W-H) method was used to calculate the size induced strain 'ε' and crystallite size t_{W-H} [10]:

$$\beta \text{ Cos } \theta = \frac{k\lambda}{t_{W-H}} + 4\varepsilon \sin\theta \quad \text{.....} \quad (2)$$

The lattice strain (ε) and average crystallite size (t_{W-H}) in Figure 2 were determined using equation (2) by linear interpolation of cos θ and sin θ. For each sample, the intercept and slope of the linear interpolation of the corresponding fitted lines of the W-H plots were used to calculate the average crystallite size and lattice strain. Figure 2 shows the W-H plots for samples A, B, and C and Table 1 shows the W-H plot results. The average crystallite size of $Ni(OH)_2$ NPs increases with increasing $Ni(NO_3)_2.6H_2O$ molarity, and the results are in perfect agreement with the results obtained by the Scherrer method, which also shows an increasing pattern with increasing $Ni(NO_3)_2.6H_2O$ content. As the molarity of $H_{12}N_2NiO_{12}$ in the study increases, the concentration of OH^- ions decreases due to the fixed molarity of NaOH. The pH of $Ni(OH)_2$ is reduced due to the decline in OH^- ions. The size and texture of the produced NPs are reportedly affected by the pH [11, 12]. It has an impact on the structural and morphological characteristics of the compound, including average crystallite size, agglomeration, strain, stress, optical band gap, and other factors. The size of $Ni(OH)_2$crystallites increases as the pH value decreases. It is a well-known literary fact that crystallite size has an inverse relationship with pH [11, 12]. Samples A and B have compressive strain, which is indicated by the negative trendlines in their W-H plots, whereas sample C has a tensile strain, which is represented by the positive trendlines in its W-H plot. The strain of samples A, B, and C increases when $Ni(NO_3)_2.6H_2O$ molarity increases. equation (2) states that the value of crystallite size is heavily influenced by lattice strain. Despite the fact that the strain is initially compressive, it changes to tensile as the molarity of $Ni(NO_3)_2.6H_2O$ is gradually increased. This increase in strain is consistent with the increase in average crystallite size because the crystallite size is smaller when compressive strain is present in the sample but increases in tensile strain occur when compressive strain continuously declines. More tension in the samples is permitted by higher tensile strain, which assists in forming crystallites. This can be understood by considering the fact that when the average crystallite size is small the several surface forces act toward the center that result in compressive strain. However, when the average crystallite size increase with increase in molarity of $Ni(NO_3)_2.6H_2O$ the surface forces relaxes by distributing the effect on larger particle surface. The relax in surface forces results change in strain from compressive to tensile. Similar investigations on the increase of average crystallite size with strain are reported in the literature [13].

Microstructural analysis

Figures 3a, 3b, 3c, respectively, show the FESEM photomicrographs of samples A, B, and C and show the typical microstructure of the samples. FESEM photomicrographs have two common characteristics. First, all of the samples have granular microstructures. The second point to remember is that the difference between the largest and smallest feature sizes is roughly 2 µm and 100 nm, respectively. The NPs are orientated erratically and are tightly bonded and nearly hexagonal in appearance the photomicrographs obtained from FESEM. Figure 3 displays the FESEM images of the synthesized nano $Ni(OH)_2$e samples with various pH values resulting from varying $Ni(NO_3)_2.6H_2O$ molarities. As seen in Figure 3, the majority of the particles have an irregular shape and range in size from 200 nm to 1.5 µm. A few particles are nearly hexagonal in shape in all the samples. When compared to sample A, which has low $Ni(NO_3)_2.6H_2O$ molarity, particles synthesized with higher $Ni(NO_3)_2.6H_2O$ molarity show uneven shape and size in Figures 3b and 3c, respectively. Additionally, the strain appears to be at a minimum in sample A. Therefore, the microstructure feature sizes in sample A should be as small as possible. A closer inspection of Figure 3a demonstrates this. Additionally, samples B and C have the highest particle strain, which contributes to the increase in particle size. The shape of NPs becomes more erratic as pH decreases. Similar research has been described in the literature [14]. Figures 3a-3c depicts the increase in particle size as the molarity of $Ni(NO_3)_2.6H_2O$ increases. The EDX spectra of the samples in figure 3a-3c reveal the elemental compositions. The EDX study validates the presence of Ni and O in the produced samples.

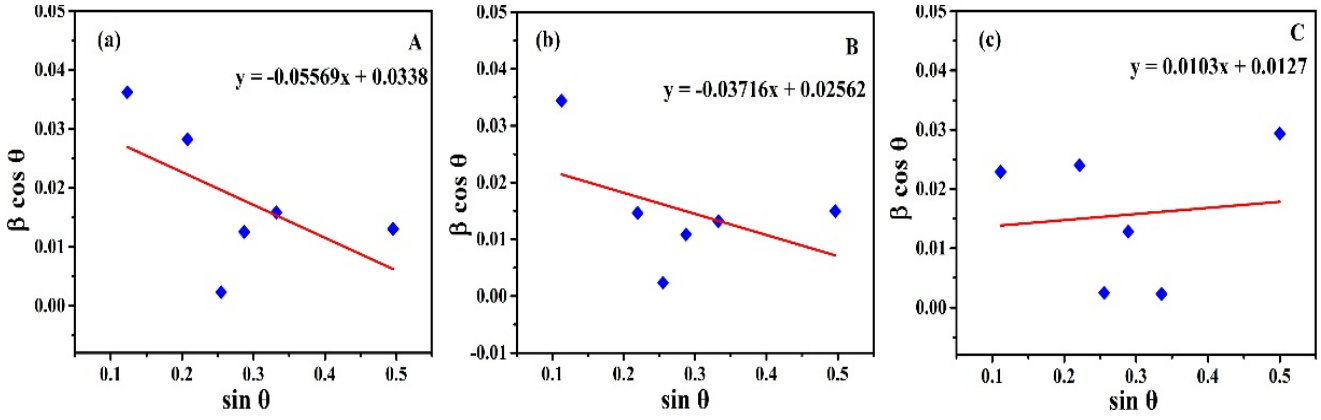

Figure 2: W–H plots of the samples (a) A, (b) B, and (c) C.

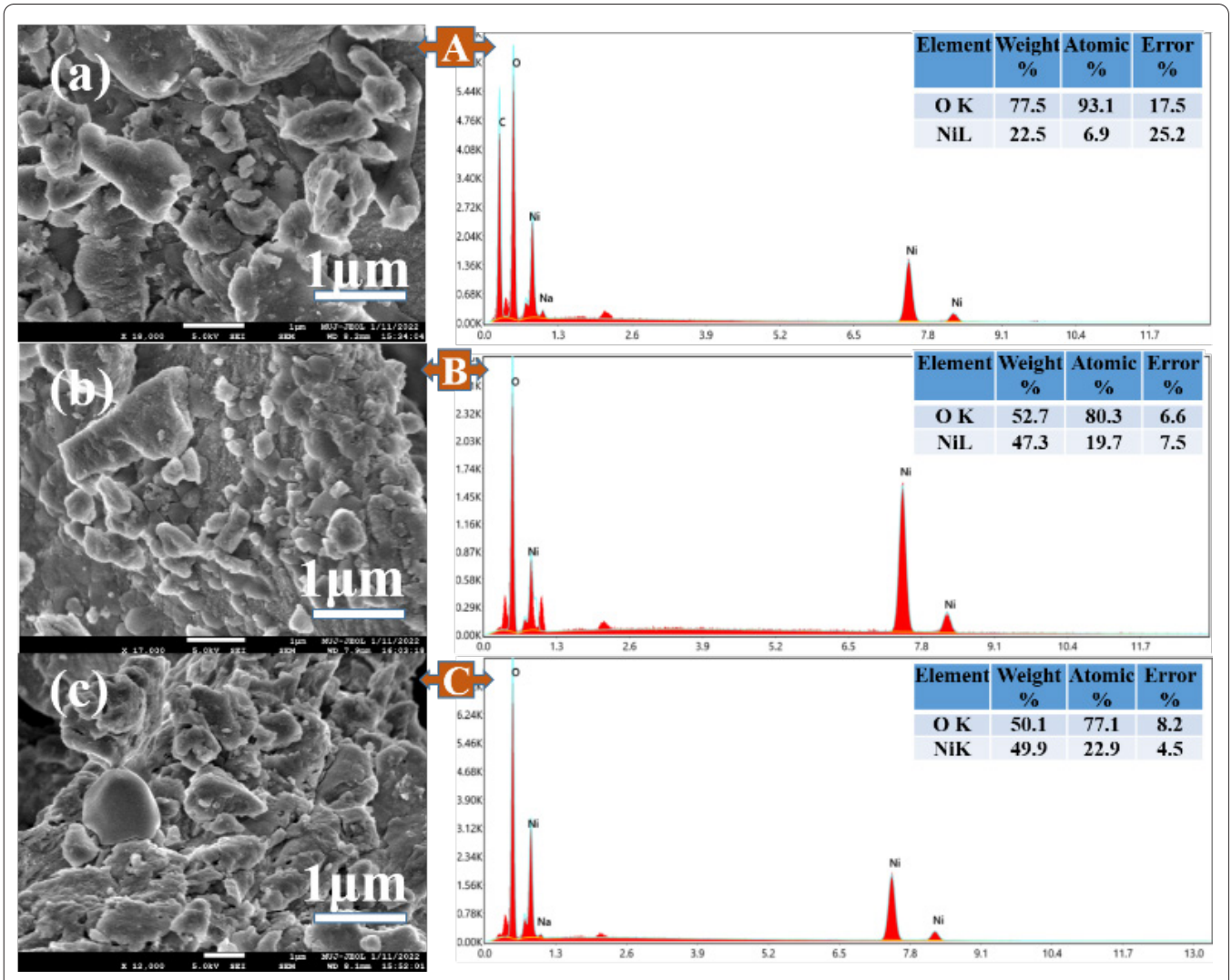

Figure 3: FESEM photomicrograph of sample (a) A, (b) B, and (c) C and their respective EDX spectra.

Surface functional group analysis

The FTIR technique outlined above is used to examine the functional groups present in the $Ni(OH)_2$ samples. Figure 4 reports the FTIR spectra outcomes for samples A, B, and C. The nearly identical FTIR spectra of samples A, B, and C confirm the presence of $Ni(OH)_2$ in all three samples. The predicted absorption bands at 3620 cm^{-1} are associated strongly with hydrogen-bound acute hydroxyl group stretching mode in water molecules. The band at 1703 cm^{-1} is the bending vibration of free water molecules, showing that water molecules are present in the as-prepared lamellar structure of β-$Ni(OH)_2$ [15]. The presence of an OH peak implies that the powder samples are primarily composed of pure hexagonal $Ni(OH)_2$ phase, as shown by the XRD data in Figure 1. The weaker absorption bands at 1297 cm^{-1} are produced by hydroxyl ion bending vibrations. In the low wavenumber range, the bands centered at 1509 cm^{-1} are associated with N-O bending vibrations. All functional groups support the research work reported in the literature [15].

Optical Analysis

The optical band gap of $Ni(OH)_2$ NPs samples were evaluated using their UV-Vis absorption characteristics. The UV-Vis spectra of the $Ni(OH)_2$ samples A, B, and C are depicted in Figure 5 as a function of wavelength. The shift of the absorption peak toward longer wavelengths produces a blue shift. This drop in pH could be the cause of the absorption bands shifting toward a shorter wavelength. Equation (3) given by Tauc's was then used to calculate the energy band gap of $Ni(OH)_2$ NPs. [16]:

$$(\alpha h\upsilon)^n = (h\upsilon - E_g).A \quad \ldots\ldots\ldots\ldots \quad (3)$$

Where n (=1/2 for a direct band gap) is a constant related to the mode of transition, α is the optical absorption coefficient, and Eg is the band gap energy. The straight portion of the curve between "hυ" and $(\alpha h\upsilon)^2$ was extrapolated in order to determine band gap energy. The band gap energies of the $Ni(OH)_2$ NPs from samples A, B, and C are 2.66 eV, 2.60 eV, and 2.58 eV, respectively, as shown in Figure 6. As the molarity of $H_{12}N_2NiO_{12}$ increases, the band gap of $Ni(OH)_2$ NPs decreases. This is expected given that Sample A with 0.4 M $Ni(NO_3)_2.6H_2O$ has a greater inherent compressive strain and, thus, a higher compressive residual stress. Other researchers [17] have observed a change in the bandgap as a result of

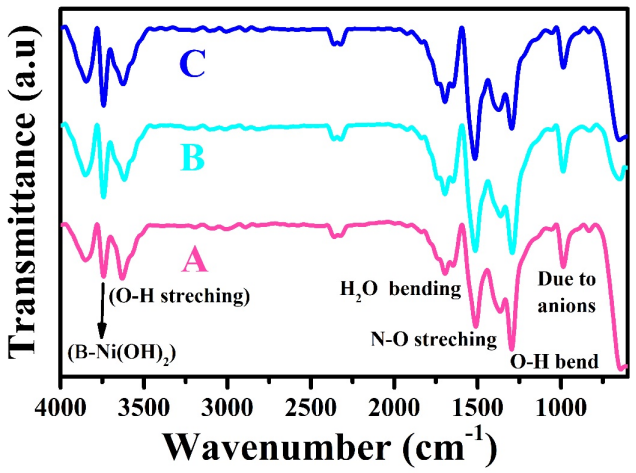

Figure 4: FTIR spectra of the samples A, B, and C.

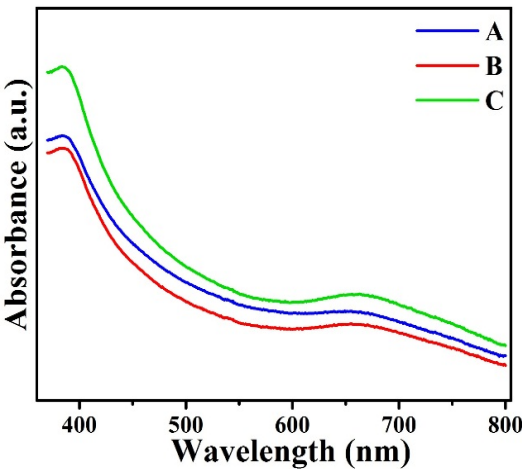

Figure 5: Absorbance spectra of the samples A, B, and C.

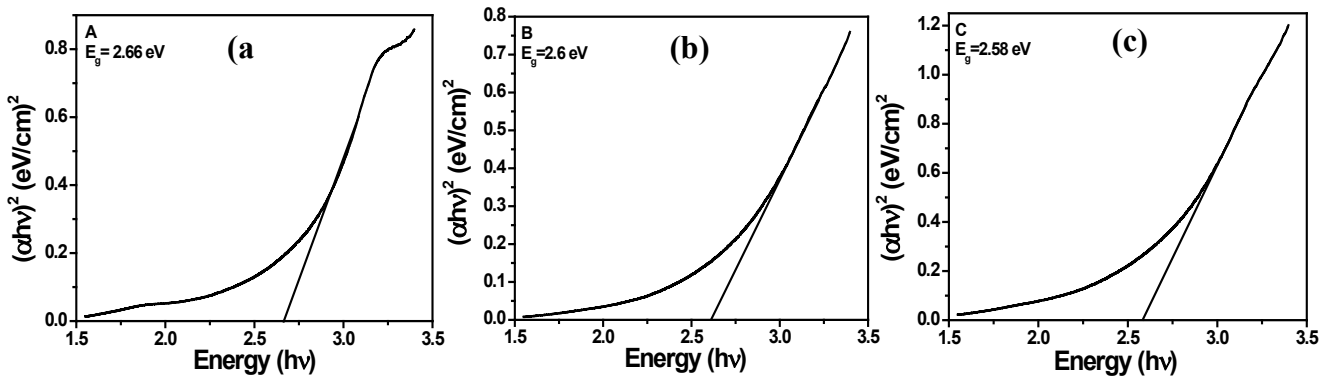

Figure 6: Tauc's plots for the samples (a) A, (b) B, and (c) C.

variations in residual stress. The XRD analysis indicates that as the pH level changes during synthesis, the particle size also changes. The band gap values of $Ni(OH)_2$ NPs are pH-dependent as well. The other investigations [16, 18] likewise noted that as pH increased, the bandgap also increased. The similar observation was observed in this study where the pH decreases with increase in molarity of $H_{12}N_2NiO_{12}$ that results in decrease of the band gap.

Conclusions

The co-precipitation technique at room temperature was effectively used to synthesize $Ni(OH)_2$ nanostructures of varied $Ni(NO_3)_2.6H_2O$ molarities, which were then examined using various characterization methods. The effect of pH on the structural, morphological, and optical properties of $Ni(OH)_2$ NPs was also investigated because changes in $Ni(NO_3)_2.6H_2O$ molarity result in pH changes. The formation of hexagonal β-$Ni(OH)_2$ is confirmed by XRD measurement. The variation in $Ni(NO_3)_2.6H_2O$ molarity was also associated with changes in average crystallite size and lattice strain. The $Ni(OH)_2$ NPs were found to have a roughly hexagonal shape with sizes ranging from 100 nm to 2 µm in FESEM photomicrographs. According to the UV-Vis study, the predicted band gap of $Ni(OH)_2$ decreases when the pH values decreases. The recent research will be helpful for interpreting the behavior of $Ni(NO_3)_2.6H_2O$ molarity variation, which may be beneficial in numerous prospective applications, including the electronics industry, storage devices, electrochemical supercapacitors, catalysts, etc.

References

1. Hall DS, Lockwood DJ, Bock C, MacDougall BR. 2015. Nickel hydroxides and related materials: a review of their structures, synthesis and properties. *Proc R Soc A* 471(2174): 20140792. https://doi.org/10.1098/rspa.2014.0792
2. Ovshinsky SR, Fetcenko MA, Ross J. 1993. Nickel metal hydride battery for electric vehicles. *Science* 260(5105): 176-181. https://doi.org/10.1126/science.260.5105.176
3. Tang Y, Liu Y, Yu S, Zhao Y, Mu S, et al. 2014. Hydrothermal synthesis of a flower-like nano-nickel hydroxide for high performance supercapacitors. *Electrochim Acta* 123: 158-166. https://doi.org/10.1016/j.electacta.2013.12.187
4. Mao N, Zhou CH, Tong DS, Yu WH, Cynthia Lin CX. 2017. Exfoliation of layered double hydroxide solids into functional nanosheets. *Appl Clay Sci* 144: 60-78. https://doi.org/10.1016/j.clay.2017.04.021
5. Oliva P, Leonardi J, Laurent JF, Delmas C, Braconnier JJ, et al. 1982. Review of the structure and the electrochemistry of nickel hydroxides and oxy-hydroxides. *J Power Sources* 8(2): 229-255. https://doi.org/10.1016/0378-7753(82)80057-8
6. Soares AL, Lorenzen AL, Schmidt A, Vidotti M. 2016. Evaluation of the electrocatalytical properties of $NiCo(OH)_2$ composite modified electrodes. *J Electroanal Chem* 765: 126-131. https://doi.org/10.1016/j.jelechem.2015.08.011

7. Xu L, Ding YS, Chen CH, Zhao L, Rimkus C, et al. 2008. 3D Flower like α-nickel hydroxide with enhanced electrochemical activity synthesized by microwave-assisted hydrothermal method. *Chem Mater* 20(1): 308-316. https://doi.org/10.1021/cm702207w
8. Mondal AK, Su D, Chen S, Sun B, Li K, et al. 2014. A simple approach to prepare nickel hydroxide nanosheets for enhanced pseudocapacitive performance. *RSC Adv* 4: 19476-19481. https://doi.org/10.1039/C4RA01719F
9. Cullity BD. 1978. Elements of x-ray diffraction. Addison-Wesley Publishing Company.
10. Harish, Kumar P, Kumari S, Debnath M, Salim A, et al. Tuning the antimicrobial efficacy of nano-Ca(OH)2 against *E. coli* using molarity. *J Mater Sci* 57: 8241-8261. https://doi.org/10.1007/s10853-022-07198-5
11. Mustapha S, Ndamitso MM, Abdulkareem AS, Tijani JO, Shuaib DT, et al. 2019. Comparative study of crystallite size using Williamson-Hall and Debye-Scherrer plots for ZnO nanoparticles. *Adv Nat Sci Nanosci Nanotechnol* 10(4): 045013. https://doi.org/10.1088/2043-6254/ab52f7
12. Sadiq SA, Waseem Z, Hanif S, Riaz S, Hayat K, et al. 2020. Investigation of the role of pH on structural and morphological properties of titanium dioxide nanoparticles. *IOP Conf Ser Mater Sci Eng* 863: 012046. https://doi.org/10.1088/1757-899X/863/1/012046
13. Harish, Kumar P, Akash, Kumari J, Kumar L, et al. 2022. Influence of chemical synthesis process on the properties of calcium hydroxide nanoparticles. *Mater Today Proc* 60(1): 153-159. https://doi.org/10.1016/j.matpr.2021.12.282
14. Alqadi MK, Abo Noqtah OA, Alzoubi F, Alzouby J, Aljarrah K. 2014. pH effect on the aggregation of silver nanoparticles synthesized by chemical reduction. *Mater Sci-Pol* 32: 107-111. https://doi.org/10.2478/s13536-013-0166-9
15. Min J, Liu J, Lei M, Wang W, Lu Y, et al. 2016. Self-assembly of parallelly aligned NiO hierarchical nanostructures with ultrathin nanosheet subunits for electrochemical supercapacitor applications. *ACS Appl Mater Interfaces* 8(1): 780-791. https://doi.org/10.1021/acsami.5b09997
16. Harish, Kumar P, Soni A, Chakinala AG, Singhal R, et al. 2022. Effect of molarity on methylene blue dye removal efficacy of nano $Ca(OH)_2$. *ChemistrySelect* 7(18): e202200393. https://doi.org/10.1002/slct.202200393
17. Harish, Kumar P, Kumari J, Phalswal P, Khanna PK, et al. 2021. Influence of impurity on the properties of chemically synthesized calcium hydroxide. *Journal of Nano- and Electronic Physics* 13(1): 01029. https://doi.org/10.21272/jnep.13(1).01029
18. Abdol Aziz RA, Abd Karim SF, Rosli NA. 2019. The effect of ph on zinc oxide nanoparticles characteristics synthesized from banana peel extract. *Key Eng Mater* 797: 271-279. https://doi.org/10.4028/www.scientific.net/KEM.797.271